Scientific Research Publishing

Engineering, 2023, 15, 75-89
https://www.scirp.org/journal/eng
ISSN Online: 1947-394X
ISSN Print: 1947-3931

Robust Radiometric Normalization of the Near Equatorial Satellite Images Using Feature Extraction and Remote Sensing Analysis

Hayder Dibs[1,2], Shattri Mansor[2], Noordin Ahmad[2,3], Nadhir Al-Ansari[4*]

[1]Water Resources Engineering Department, Faculty of Engineering, Al-Qasim Green University, Al-Qasim, Iraq
[2]Faculty of Engineering, Geospatial Information Science Research Centre, Department of Civil Engineering, University Putra Malaysia, Selangor, Malaysia
[3]National Space Agency Malaysia (ANGKASA), Kementerian Sains, Teknologi dan Inovasi, Pusat Angkasa Negara, Banting, Malaysia
[4]Department of Civil Environmental and Natural Resources Engineering, Lulea University of Technology, Lulea, Sweden
Email: Dr.hayderdibs@wrec.uoqasim.edu.iq, haiderdibs@gmal.com, shattri@upm.edu.my, noordin.ahmad@gmail.com, *nadhir.alansari@ltu.se

How to cite this paper: Dibs, H., Mansor, S., Ahmad, N. and Al-Ansari, N. (2023) Robust Radiometric Normalization of the Near Equatorial Satellite Images Using Feature Extraction and Remote Sensing Analysis. *Engineering*, **15**, 75-89.
https://doi.org/10.4236/eng.2023.152007

Received: January 18, 2023
Accepted: February 13, 2023
Published: February 16, 2023

Abstract

Relative radiometric normalization (RRN) minimizes radiometric differences among images caused by inconsistencies of acquisition conditions rather than changes in surface. Scale invariant feature transform (SIFT) has the ability to automatically extract control points (CPs) and is commonly used for remote sensing images. However, its results are mostly inaccurate and sometimes contain incorrect matching caused by generating a small number of false CP pairs. These CP pairs have high false alarm matching. This paper presents a modified method to improve the performance of SIFT CPs matching by applying sum of absolute difference (SAD) in a different manner for the new optical satellite generation called near-equatorial orbit satellite and multi-sensor images. The proposed method, which has a significantly high rate of correct matches, improves CP matching. The data in this study were obtained from the RazakSAT satellite a new near equatorial satellite system. The proposed method involves six steps: 1) data reduction, 2) applying the SIFT to automatically extract CPs, 3) refining CPs matching by using SAD algorithm with empirical threshold, and 4) calculation of true CPs intensity values over all image' bands, 5) preforming a linear regression model between the intensity values of CPs locate in reverence and sensed image' bands, 6) Relative radiometric normalization conducting using regression transformation functions. Different thresholds have experimentally tested and used in conducting this study (50 and 70), by followed the proposed method, and it removed the false extracted SIFT CPs to be from 775, 1125, 883, 804, 883 and 681 false pairs to

342, 424, 547, 706, 547, and 469 corrected and matched pairs, respectively.

Keywords

Relative Radiometric Normalization, Scale Invariant Feature Transform, Automatically Extraction Control Points, Sum of Absolute Difference

1. Introduction

Radiometric normalization aims to reduce the radiation differences between images by adjusting the color of each image. Radiometric normalization correction on remote sensing imagery has two techniques: absolute radiometric normalization and relative radiometric normalization [1] [2] [3]. The first technique requires data be collected in the same time of imaging through in situ work [4]. The second technique does not require data to be collected in the same time of image capturing [5] [6]. According to the previous works no single approach has a universal application and is able to overcome radiometric normalization because solutions are dependent on locations, applications, and images [7]-[13]. Analysts must therefore be aware of existing procedures, be prepared to use or modify these, or develop alternative procedures [14]. Pseudo invariant features (PIFs) refer to radiometric truth control points that should exhibit no significant change between acquisition dates [12] [13] [15]. Many previous studies have addressed the selection of PIFs to perform relative radiometric normalization [7] [16]. Some researchers performed relative radiometric normalization (RRN) manually, whereas others performed it automatically [17] [18]. Most researchers performed RRN on a remotely sensed image [13] [19] [20], involved several image bands, and applied regression between images directly. However, a poor result was achieved in terms of finding the most accurate PIFs compared with the result obtained from involving all image bands in the regression [15] [21] [22] [23] [24] [25]. Scenes of the same target area acquired at different times have been nearly impossible to compare without performing image normalization because of variations in atmospheric conditions, look/view angles, or sensor parameters that occur between acquisition time and illumination [26] [27]. Even visual comparison of these images may be difficult [28].

In early studies, remote sensing imagery was both expensive and difficult to obtain [29]-[34]. However, currently, many images can be obtained from practically any region in the world provided for free by the LANDSAT project. Scott *et al.* [28] studied two different scenarios in which three and two images were used, respectively. In the study of Hall [18], a total of six images were used. Yuan and Elvidge [35] compared six different RRN algorithms by using a total of two images. Song *et al.* [36] employed seven images, and Baisantry *et al.* [26] used only three. Canty *et al.* [37] studied two different scenarios in which five and two images were used, respectively.

The most recent study [27] employed only five images. A common measure of

performance, which was used by Scott *et al.* [28], Hall, [18], Yuan and Elvidge [35], and Qian *et al.* [38], is the MSE of the values of the PIFs after RRN and their values in the control image. However, the PIFs or no-change points are defined subjectively within the same algorithm that is being evaluated. Moreover, the MSE measure is inconsistent with any of the approaches because none of them propose to obtain the linear regression parameters by optimizing the MSE over the no-change locations. Song *et al.* [36] proposed an arguably more specific but consistent approach to performance assessment and employed crossed classification results both from the control image to the corrected image and vice versa. This article is organized as follows: section 2 shows the Methodology, Study Area description, dataset collecting. Section 3 demonstrates the datasets processing and analyzing steps, explains the RRN and quantitative assessment method. Section 4 mainly proves the effectiveness of our proposed method and analyzes the RRN performance. Section 5 discusses the RNN performance in different ground features. Finally, section 6 concludes this work. This research will help the researchers and analysts to overcome with the problem of 1) can not process or analysis datasets captured for same study area but in different time and illumination, 2) they can not use different datasets captured by multi-sensor. Analysts will be able to study and investigate different remote sensing applications in tropical areas around the world have these problems to study such as: land use and land cover, change detection, forest and environment monitoring and management and so on.

2. Methodology

In this research, we work on relative radiometric normalizing on images have same features but with different intensity values. The proposed method is combining the RI-SIFT method [20] and integrate with determine intensity values method to calculate the PIFs over each band of the reference and sensed images of each pixel, by inputting both of the reference and sensed images into RI-SIFT method to determine the most accurate locations of CPs in each band of the reference and sensed images. Then it calculated the intensity values of this CPs and this CPs considers as RRN-PIFs in this research. The developed method of finding the PIFs for this research we are called a "PIFs-SIFT" technique. **Figure 1** illustrates the processing steps of extracting the RRN-PIFs technique.

2.1. Study Area Description

The study area was at the campus of University Putra Malaysia (UPM). The UPM University is located in Selangor state, Central Peninsular Malaysia close to the capital city, Kuala Lumpur, and next to Malaysia's administrative capital city, Putrajaya. It is one of the Malaysian research universities. **Figure 2** shows the location of the UPM University.

2.2. Dataset LAB Collecting

The datasets were collected during lab work for this research, it was performed

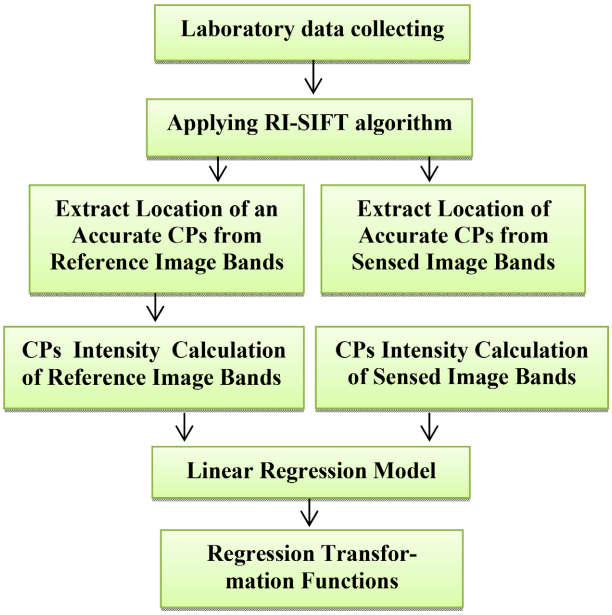

Figure 1. Flowchart of proposed method.

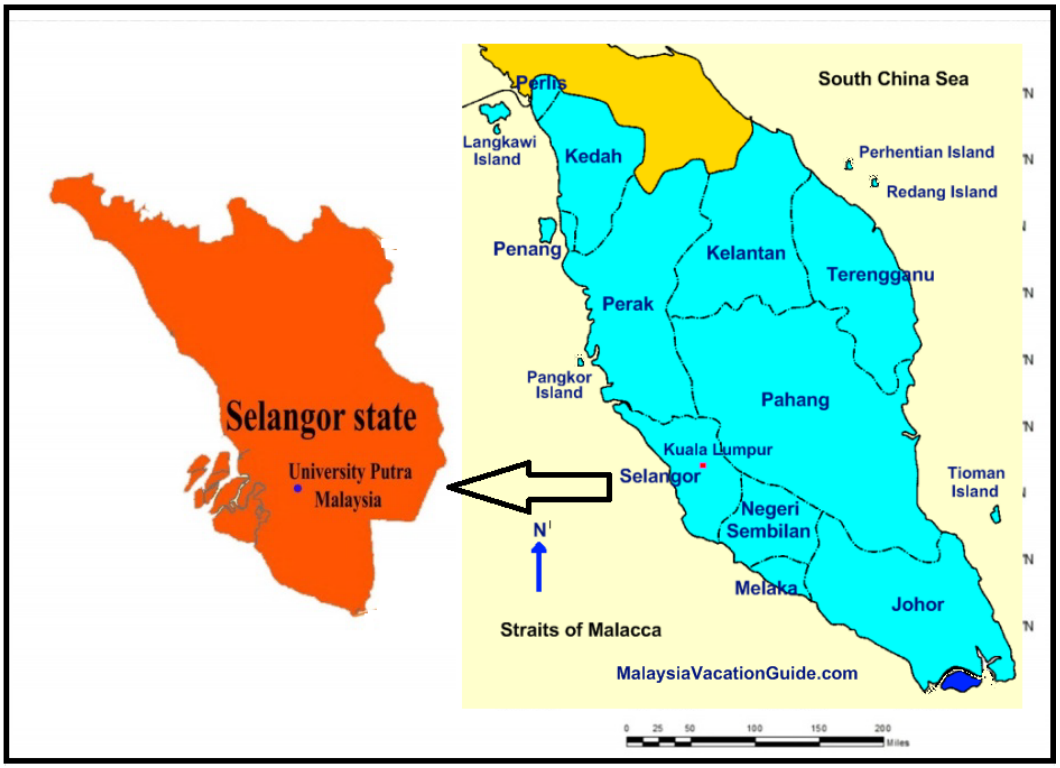

Figure 2. Study area in UPM campus.

at the Geospatial Information Science Research Center (GISRC) laboratory of Faculty of Engineering in UPM University. The images were collected by using the invented and designed goniometer for this work [20] to simulate the Near Equatorial Satellite system (NEqO) images. Figure 3 shows the used goniometer device.

Figure 3. The invented goniometer.

Laboratory work was conducted to simulate and capture images at night to avoid different reflectance levels coming from the laboratory windows. Seven images were collected, each one with a different illumination intensity than the others. The captured images were used in performing RRN and to simulate the NEqO satellite system. Sample of features captured in these images are soil, stone, cement, vegetation, and rocks represent real-world features in any real location [39]. All the images were captured with the same specifications but different illumination levels. The optical sensor used in this study is an optical Canon SX700H Power Shot camera, and the illumination source is a 150 w QTH. Figure demonstrates the arrangement before image capture. **Figure 4** shows laboratory arrangements before image capturing.

3. Dataset Analysis

Most studies that analyzed the relative radiometric correction of multi-temporal images regarded the image captured at noon time as the reference image for normalizing other images. The sun at noon is at the highest altitude in its orbital and illumination degree; all features located in the image exhibit the real reflectance at that time [5] [40]. Therefore, six images were selected as slave images and one image was selected as the reference image for normalizing the six images. The reference image has the highest light intensity value and is considered the image captured at noon. **Figure 5** shows the captured images at the GISRC lab of UPM. All slave images were registered with respect to the reference image. The images were registered on the basis of the image coordinate system. The coordinate system is used to place elements in relation to one another, and the user can use it to define elements and position them in relation to one another [40]. In this stage, the origin point (0, 0) at the left upper corner of the reference image was considered. All the images are in JPEG format in RGB color. Grayscale conversion and image compression were performed to significantly reduce

Figure 4. The laboratory arrangements to capture the images.

(a) (b)

Figure 5. Collected images at different illumination level, (a) the reference image, (b) the six sensed images in different illumination.

the processing time and storage requirements. Image compression was used to minimize image sizes based on previous studies [41] [42].

The next steps applied the proposed PIFs-SIFT method was; First RI-SIFT method was employed to extract the most invariant CPs to any change in illumination, rotation, starching, and scaling (Hayder *et al.* 2020a). **Figures 6-8** show run the RI-SIFT method using programmed Graphic User Interface (GUI) in Matlab software with the thresholds to extract the CPs. Second, the SAD algorithm and an empirical threshold were employed in the RI-SIFT method to extract the most accurate invariant CPs and remove the incorrect matched CPs. In addition, the accurate invariant CPs has invariant intensity. Third, the next step was calculated the value of this CPs to use in RRN as control points of relative

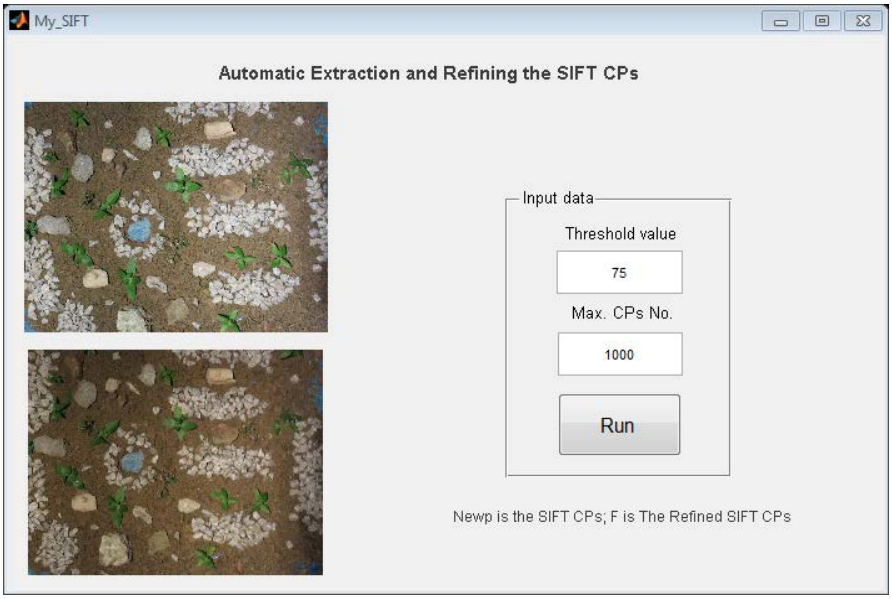

Figure 6. The RI-SIFT CPs Extraction.

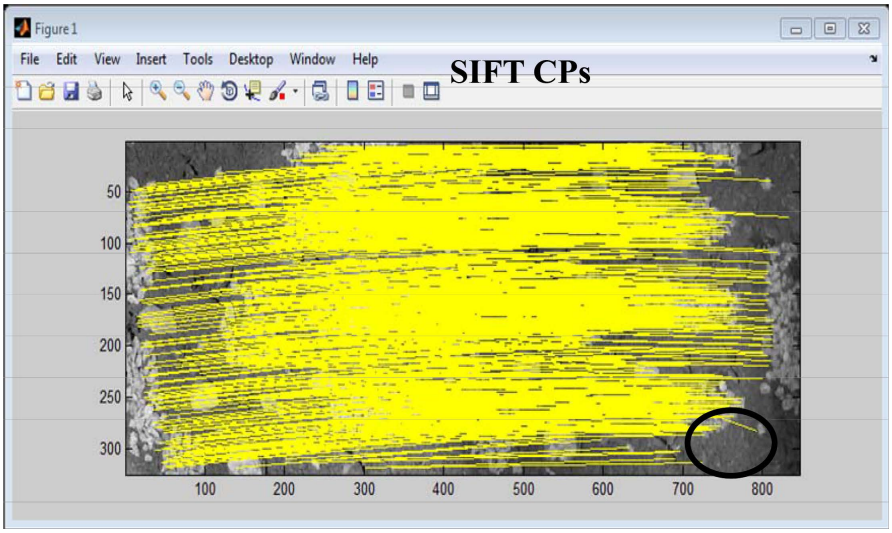

Figure 7. SIFT results.

radiometric normalization. The intensity values of these radiometric control points is the true reflectance control points of the reference and slave image bands, the intensity value of CPs calculated using formula below:

$$v(x,y) = a_{xy} \tag{1}$$

where (x, y) denote the coordinate system of the location to which we wish to assign an intensity value (a point of the grid). a_{xy} is the intersection of x and y. We let $v(x,y)$ denote the intensity value obtained from using the following mathematical expression [40]:

Figure 7 shows the CPs and their matching lines in yellow color. It also demonstrates one CP pair as false CPs with an incorrect match, as indicated by the black circle in right side of Figure 7. Therefore, the extracted CPs should be re-

fined to remove the incorrect matches and obtain accurate CPs. However, Figure 8 indicates the reference and slave images after remove the false CPs, from using the SAD algorithm. This step was performed automatically using the GUI.

Figure 8 illustrates the most accurate CPs after removing the false CPs and decreasing the CP number based on the threshold used for the images. The empirical threshold that we used to remove the false CPs was 75 as indicates in Figure 6. Table 1 shows the illumination intensity, empirical threshold, and number of extracted SIFT CPs and refined CPs.

Table 1 shows the decrease in the number of extracted SIFT CPs. The first refinement was conducted between image-1 (slave image) and the reference image. The empirical threshold used to refine the CPs was 75. However, the threshold value for images 2, 3, and 4 was 50. Images 5 and 6 used different thresholds to refine their CPs (*i.e.* 75 and 100, respectively). The number of extracted CPs largely decreased. First, the SIFT CP number between image-1 and the reference image was 775, but this number decreased to 342 after applying SAD. This condition was similarly observed in the other images. The refined CPs were used in the next stage to extract the brightness value of each CP from the reference and slave images.

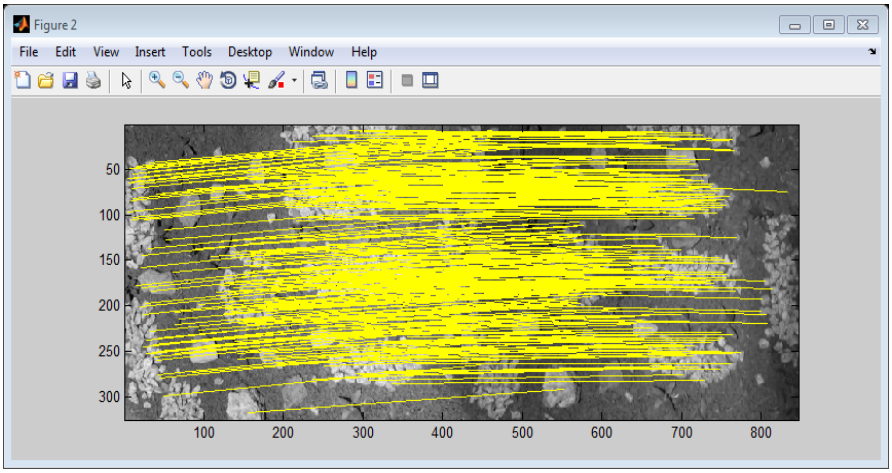

Figure 8. Removing false CPs from the reference and slave images.

Table 1. Shows threshold, SIFT CPs, and RI-SIFT-CPs.

Images	Light intensity	Threshold	SIFT CPs	RI-SIFT CPs
1	Low	75	775	342
2	Moderate	50	1125	424
3	Higher	50	883	547
Noon	Highest (Noon)	Noon	Noon	Noon
4	Less than Noon	50	804	706
5	Moderate	75	883	547
6	Lowest	100	681	469

3.1. Intensity Values Calculation

After identifying the most accurate CPs locations by using RI-SIFT from the reference and slave images. In this step determines the intensity values of the CPs automatically for each band of the reference and slave images. Calculation of the intensity value of each extracted CPs for all bands of the reference and slave images were based on Equation (1) mentioned above. It was conducted using MatLab environment. The output of this step is shown in Table 2 that contains samples of the intensity values of all bands of the reference and slave images. All the calculated intensity values over the bands were regarded as PIFs to use in performing RRN between the reference and sensed images in the next stage.

3.2. Liner Regression Model

In this stage of the relative radiometric normalization the linear regression was performed between the PIFs of the reference image bands with the corresponding slave image bands in order to find how match the bands in reference and sensed image has intensity equal and/or near to each PIFs in the images. The linear regression was conducted by using Microsoft Excel. The output of the linear regression model was established 18 equations between each reference image bands and corresponding slave image bands. Each equation was used to normalize the sensed image's band to those in reference image. The eighteen regression functions were obtained after performing linear regression. Table 3 illustrates the 18 transformation functions of linear regression. The Band Math tool under the ENVI software was used to perform the transformation between the bands. The next step was applying layer stacking to obtain the final normalized

Table 2. Intensity values of the reference and slave image bands.

Red	Green	Blue	RED	Green	Blue
89	80	63	36	26	14
89	80	63	36	26	14
78	71	55	92	77	54
92	80	64	107	94	78
81	70	52	52	85	30
84	76	55	77	69	50
83	74	57	86	75	57
89	81	62	76	68	49
78	73	54	41	68	29
98	91	75	78	72	50
96	84	62	85	74	54
81	68	52	76	65	45

Table 3. Linear Regression transformation Functions.

Image no.	Regression function to reference image bands
image-1	
Red-band	y = 0.046x + 114.710
Green-band	y = 0.0422x + 104.48
Blue-band	y = 0.0156x + 91.933
image-2	
Red-band	y = 0.0888x + 66.725
Green-band	y = 0.0564x + 72.888
Blue-band	y = 0.1021x + 62.407
image-3	
Red-band	y = 0.0526x + 121.77
Green-band	y = 0.2047x + 95.387
Blue-band	y = 0.1845x + 91.166
image-4	
Red-band	y = 0.0723x + 96.614
Green-band	y = 0.0087x + 78.760
Blue-band	y = 0.0348x + 66.004
image-5	
Red-band	y = 0.020x + 69.5070
Green-band	y = 0.0435x + 65.039
Blue-band	y = 0.0724x + 48.270
image-6	
Red-band	y = 0.1526x + 83.517
Green-band	y = 0.1425x + 89.239
Blue-band	y = 0.0745x + 59.269

slave images as RGB. Figure 9 shows the images after normalization

4. Conclusion

Relative radiometric normalization is one of the common problems in processing and analyzing different image captured same the study area but captured in different times of the day such as images obtained from multi-sensor and the NE-qO satellite images. The datasets were collected using goniometer in the Lab of UPM University. The proposed technique used the RI-SIFT algorithm to extract correct CPs automatically and then calculate the intensity values of this CPs over the seven images' bands to extract the PIFs. These PIFs were adopted to perform the relative radiometric normalization. The PIFs in this research exhibit truthful

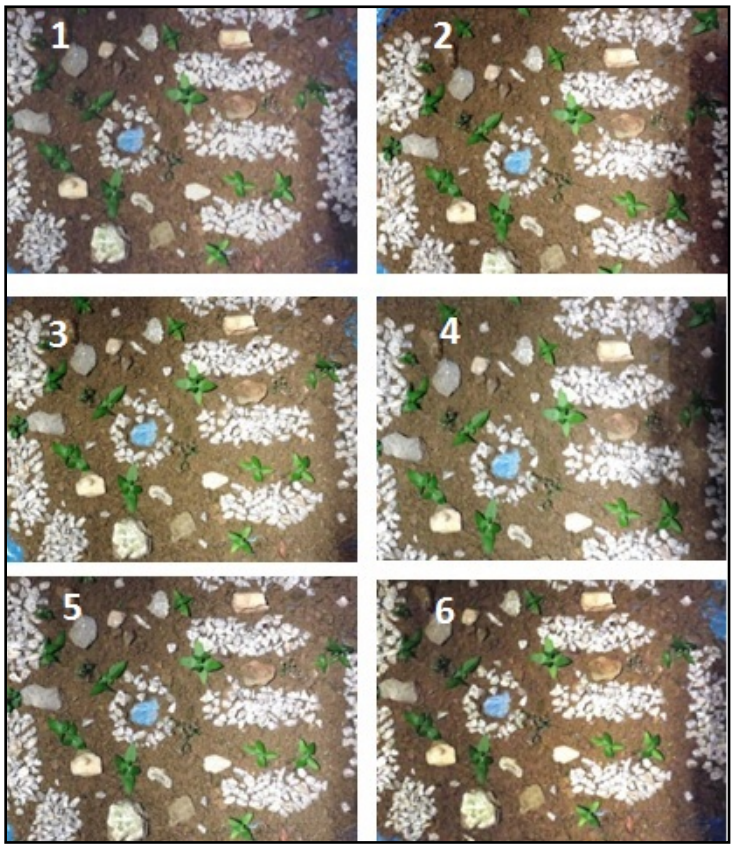

Figure 9. All normalized images.

reflectance of the most invariant features to any changes in stretching, illumination, and rotation in both the reference and sensed image bands. The proposed method shows promising results that can help analysts and researchers to apply it in their research that deals with multi-temporal and multi-sensor and NEqO images. Different thresholds have experimentally tested and used in conducting this study (50 and 70), by followed the proposed method, and it removed the false extracted SIFT CPs to be from 775, 1125, 883, 804, 883 and 681 false pairs to 342, 424, 547, 706, 547, and 469 corrected and matched pairs, respectively.

Declarations

Author Contributions

Conceptualization, HD, SM, NA and NAA; methodology, HD, SM, NA and NAA; software, HD and SM, NA; validation, HD, and NAA; investigation, HD, and NAA; data curation, HD, SM, and NA; writing-original draft preparation, HD, SM, NA. and NAA; visualization, NAA; project administration, NAA. All authors have read and agreed to the published version of the manuscript.

Data Availability Statement

Data available on request due to restrictions, the data presented in this study are available on request from the corresponding author. The data are not publicly

available due to it relate to AL-Qasim Green University.

Acknowledgments

Authors would like to acknowledge the insightful contributions of the anonymous reviewers. The authors also would like to express their thankfulness to the AL-Qasim Green University, University Putra Malaysia (Malaysia), Lulea University of Technology (Sweden) for the support provided to accomplish this study.

Conflicts of Interest

The authors declare no conflicts of interest regarding the publication of this paper.

References

[1] Hasab, H.A., Jawad, H.A., Dibs, H., Hussain, H.M. and Al-Ansari, N. (2020) Evaluation of Water Quality Parameters in Marshes Zone Southern of Iraq Based on Remote Sensing and GIS Techniques. *Water, Air, & Soil Pollution*, **231**, Article No. 183. https://doi.org/10.1007/s11270-020-04531-z

[2] Dibs, H., Mansor, S., Ahmad, N., Pradhan, B. and Al-Ansari, N. (2020) Automatic Fast and Robust Technique to Refine Extracted SIFT Key Points for Remote Sensing Images. *Journal of Civil Engineering and Architecture*, **14**, 339-350. https://doi.org/10.17265/1934-7359/2020.06.005

[3] Dibs, H., Hasab, H.A., Al-Rifaie, J.K. and Al-Ansari, N. (2020) An Optimal Approach for Land-Use/Land-Cover Mapping by Integration and Fusion of Multispectral Landsat OLI Images: Case Study in Baghdad, Iraq. *Water, Air, & Soil Pollution*, **231**, Article No. 488. https://doi.org/10.1007/s11270-020-04846-x

[4] Dibs, H., Hasab, H.A., Jaber, H.S. and Al-Ansari, N. (2021) Automatic Feature Extraction and Matching Modelling for Highly Noise Near-Equatorial Satellite Images. *Innovative Infrastructure Solutions*, **7**, Article No. 2. https://doi.org/10.1007/s41062-021-00598-7

[5] Richards, J.A. (2013) Remote Sensing Digital Image Analysis. Springer-vertag, Berlin. https://doi.org/10.1007/978-3-642-30062-2

[6] Hasab, H.A., Dibs, H., Dawood, A.S., Hadi, W.H., Hussain, H.M. and Al-Ansari, N. (2020) Monitoring and Assessment of Salinity and Chemicals in Agricultural Lands by a Remote Sensing Technique and Soil Moisture with Chemical Index Models. *Geosciences*, **10**, 207. https://doi.org/10.3390/geosciences10060207

[7] Seo, D.K., Kim, Y.H., Eo, Y.D., Park, W.Y. and Park, H.C. (2017) Generation of Radiometric, Phenological Normalized Image Based on Random Forest Regression for Change Detection. *Remote Sensing*, **9**, Article No. 1163. https://doi.org/10.3390/rs9111163

[8] Dibs, H., Mansor, S., Ahmad, N. and Pradhan, B. (2014) Registration Model for Near-Equatorial Earth Observation Satellite Images Using Automatic Extraction of Control Points. *International Symposium and Exhibition on Geoinformation*, Volume 3, 2184-2200. https://doi.org/10.1080/01431161.2015.1034891

[9] Zhang, L., Wu, C. and Du, B. (2014) Automatic Radiometric Normalization for Multitemporal Remote Sensing Imagery with Iterative Slow Feature Analysis. *IEEE Transactions on Geoscience and Remote Sensing*, **52**, 6141-6155.

https://doi.org/10.1109/TGRS.2013.2295263

[10] Dibs, H. (2018) Comparison of Derived Indices and Unsupervised Classification for AL-Razaza Lake Dehydration Extent Using Multi-Temporal Satellite Data and Remote Sensing Analysis. *Journal of Engineering and Applied Science*, **13**, 1-8.

[11] Dibs, H., Al-Hedny, S. and Karkoosh, H.A. (2018) Extracting Detailed Buildings 3D Model with Using High Resolution Satellite Imagery by Remote Sensing and GIS Analysis; Al-Qasim Green University a Case Study. *International Journal of Civil Engineering and Technology*, **9**, 1097-1108.

[12] Moghimi, A., Mohammadzadeh, A., Celik, T. and Amani, M. (2020) A Novel Radiometric Control Set Sample Selection Strategy for Relative Radiometric Normalization of Multitemporal Satellite Images. *IEEE Transactions on Geoscience and Remote Sensing*, **59**, 2503-2519. https://doi.org/10.1109/TGRS.2020.2995394

[13] Liu, K., Ke, T., Tao, P., He, J., Xi, K. and Yang, K. (2020) Robust Radiometric Normalization of Multitemporal Satellite Images via Block Adjustment without Master Images. *IEEE Journal of Selected Topics in Applied Earth Observations and Remote Sensing*, **13**, 6029-6043. https://doi.org/10.1109/JSTARS.2020.3028062

[14] Jason, T.C. and John, P.K. (2009) Mis-Registration Impacts on Hyperspectral Target Detection. *Journal of Applied Remote Sensing*, **3**, Article ID: 033513.

[15] Dibs, H., Mansor, S., Ahmad, N. and Pradhan, B. (2015) Band-to-Band Registration Model for Near-Equatorial Earth Observation Satellite Images with the Use of Automatic Control Point Extraction. *International Journal of Remote Sensing*, **36**, 2184-2200. https://doi.org/10.1080/01431161.2015.1034891

[16] Dibs, H. and Hussain, T.H. (2018) Estimation and Mapping the Rubber Trees Growth Distribution Using Multi Sensor Imagery with Remote Sensing and GIS Analysis. *Journal of University of Babylon for Pure and Applied Sciences*, **26**, 109-123.

[17] Schott, J.R., Salvaggio, C. and Volchok, W.J. (1988) Radiometric Scene Normalization Using Pseudo Invariant Features. *Remote Sensing of Environment*, **26**, 1-16. https://doi.org/10.1016/0034-4257(88)90116-2

[18] Hall, F.G., Strebel, D.E., Nickeson, J.E. and Goetz, S.J. (1991) Radiometric Rectification: Toward a Common Radiometric Response among Multidate, Multisensor Images. *Remote Sensing of Environment*, **35**, 11-27. https://doi.org/10.1016/0034-4257(91)90062-B

[19] Allan, A.N. (2011) Kernel Maximum Autocorrelation Factor and Minimum Noise Fraction Transformations. *IEEE Transactions on Image Processing*, **20**, 612-624. https://doi.org/10.1109/TIP.2010.2076296

[20] Dibs, H., Mansor, S., Ahmadb, N. and Al-Ansari, N. (2020) Simulate New Near Equatorial Satellite System by a Novel Multi-Fields and Purposes Remote Sensing Goniometer. *Engineering*, **12**, 325-346. https://doi.org/10.4236/eng.2020.126026

[21] Morton, J.C. Allan, A.N. (2008) Automatic Radiometric Normalization of Multitemporal Satellite Imagery with the Iteratively Re-Weighted MAD Transformation. *Remote Sensing of Environment*, **112**, 1025-1036. https://doi.org/10.1016/j.rse.2007.07.013

[22] Carlos, J., Broncano, M., Carlos, P.R., Rubén, G.C., Andrés, C.S., Brown, M. and Lowe, D.G. (2010) Invariant Features from Interest Point Groups. *Machine Vision Conference*, Cardiff, 2-5 September 2002, 656-665.

[23] Fahad, K.H., Hussein, S. and Dibs, H. (2020) Spatial-Temporal Analysis of Land Use and Land Cover Change Detection Using Remote Sensing and GIS Techniques. *IOP Conference Series: Materials Science and Engineering*, **671**, 12-46.

https://doi.org/10.1088/1757-899X/671/1/012046

[24] Hashim, F., Dibs, H. and Jaber, H.S. (2021) Applying Support Vector Machine Algorithm on Multispectral Remotely Sensed Satellite Image for Geospatial Analysis. *Journal of Physics*: *Conference Series*, **1963**, Article ID: 012110. https://doi.org/10.1088/1742-6596/1963/1/012110

[25] Dibs, H. and Al-Hedny, S. (2019) Detection Wetland Dehydration Extent with Multi-Temporal Remotely Sensed Data Using Remote Sensing Analysis and GIS Techniques. *International Journal of Civil Engineering and Technology*, **10**, 143-154.

[26] Baisantry, M., Negi, D. and Manocha, O. (2012) Automatic Relative Radiometric Normalization for Change Detection of Satellite Imagery. *International Journal on Information Technology*, **2**, 116-124.

[27] Connell, J., Connolly, J., Vermote, E.F. and Holden, N.M. (2013) Radiometric Normalization for Change Detection in Peatlands: A Modified Temporal Invariant Cluster Approach. *International Journal of Remote Sensing*, **34**, 2905-2924. https://doi.org/10.1080/01431161.2012.752886

[28] Hashim, F., Dibs, H. and Jaber, H.S. (2022) Adopting Gram-Schmidt and Brovey Methods for Estimating Land Use and Land Cover Using Remote Sensing and Satellite Images. *Nature Environment and Pollution Technology*, **21**, 867-881. https://doi.org/10.46488/NEPT.2022.v21i02.050

[29] Sadeghi, V., Ebadi, H. and Ahmadi, F.F. (2013) A New Model for Automatic Normalization of Multi-Temporal Satellite Images Using Artificial Neural Network and Mathematical Methods. *Applied Mathematical Modelling* **37**, 6437-6445. https://doi.org/10.1016/j.apm.2013.01.006

[30] Nazeer, M., Wong, M.S. and Nichol, J.E. (2017) A New Approach for the Estimation of Phytoplankton Cell Counts Associated with Algal Blooms. *Science of the Total Environment*, **5**, 125-138. https://doi.org/10.1016/j.scitotenv.2017.02.182

[31] Dibs, H., Idrees, M.O., Saeidi, V. and Mansor, S. (2016) Automatic Keypoints Extraction from UAV Image with Refine and Improved Scale Invariant Features Transform (RI-SIFT). *International Journal of Geoinformatics*, **12**, 51-58.

[32] Huang, L.T., Jiao, W.L., Long, T.F. and Kang, C.L. (2020) A Radiometric Normalization Method of Controlling No-Changed Set (CNCS) for Diverse Landcover Using Multi-Sensor Data. *The International Archives of the Photogrammetry, Remote Sensing and Spatial Information Sciences*, **3**, 863-870. https://doi.org/10.5194/isprs-archives-XLII-3-W10-863-2020

[33] Dibs, H., Hasab, H.A., Mahmoud, A.S. and Al-Ansari, N. (2021) Fusion Methods and Multi-Classifiers to Improve Land Cover Estimation Using Remote Sensing Analysis. *Geotechnical and Geological Engineering*, **39**, 5825-5842. https://doi.org/10.1007/s10706-021-01869-x

[34] Moghimi, A., Sarmadian, A., Mohammadzadeh, A., Celik, T., Amani, M. and Kusetogullari, H. (2021) Distortion Robust Relative Radiometric Normalization of Multitemporal and Multisensor Remote Sensing Images Using Image Features. *IEEE Transactions on Geoscience and Remote Sensing*, **60**, Article ID: 5400820. https://doi.org/10.1109/TGRS.2021.3063151

[35] Yuan, D. and Elvidge, C.D. (1996) Comparison of Relative Radiometric Normalization Techniques. *ISPRS Journal of Photogrammetry and Remote Sensing*, **51**, 117-126. https://doi.org/10.1016/0924-2716(96)00018-4

[36] Song, C., Woodcock, C.E., Seto, K.C., Lenney, M.P. and Macomber, S.A. (2001) Classification and Change Detection Using Landsat TM Data: When and How to Correct Atmospheric Effects. *Remote Sensing of Environment*, **75**, 230-244.

https://doi.org/10.1016/S0034-4257(00)00169-3

[37] Canty, M.J., Nielsen, A.A. and Schmidt, M. (2004) Automatic Radiometric Normalization of Multi-Temporal Satellite Imagery. *Remote Sensing of Environment*, **91**, 441-451. https://doi.org/10.1016/j.rse.2003.10.024

[38] Qian, D., Nareenart, R., Aksuntorn, A.O. and Lori, M.B. (2008) Automatic Registration and Mosaicking for Airborne Multispectral Image Sequences. *Photogrammetric Engineering & Remote Sensing*, **74**, 169-181. https://doi.org/10.14358/PERS.74.2.169

[39] Loon, H., Thomas, W. and fltzHugh, A. (2000) Standardized Radiometric Normalization Method for Change Detection Using Remotely Sensed Imagery. *Photogrammetric Engineering & Remote Sensing*, **66**, 173-181.

[40] Gonzalez, R.C. and Woods, R.E. (2008) Digital Image Processing. 3rd Edition, Pearson Prentice, London.

[41] Chureesampant, K. and Susaki, J. (2012) Automatic Unsupervised Change Detection Using Multi-Temporal Polarimetric SAR Data. *IEEE International Geoscience and Remote Sensing Symposium*, **1**, 6192-6195. https://doi.org/10.1109/IGARSS.2012.6352671

[42] Chureesampant, K. and Susaki, J. (2014) Automatic GCP Extraction of Fully. *Geoscience and Remote Sensing*, *IEEE Transactions*, **52**, 137-148. https://doi.org/10.1109/TGRS.2012.2236890